Journal of Zhejiang University-SCIENCE A (Applied Physics & Engineering) 2025 26(3):266-276
www.jzus.zju.edu.cn; www.springer.com/journal/11582
E-mail: jzus_a@zju.edu.cn

Research Article

https://doi.org/10.1631/jzus.A2300546

Parametric design for the valve seat of a high-temperature and high-pressure valve inside wind tunnels

Fengwei HOU[1], Haifeng SHU[1], Binbin WU[2], Chengliang YU[2], Zhehui MA[3], Wenqing LI[4]✉, Jinyuan QIAN[3]

[1]*Hypervelocity Aerodynamics Institute, China Aerodynamics Research and Development Center, Mianyang 621000, China*
[2]*Shanghai Koko Valve Group Co., Ltd., Shanghai 201802, China*
[3]*Institute of Advanced Equipment, Zhejiang University, Hangzhou 310027, China*
[4]*State Key Laboratory of Fluid Power Components and Mechatronic Systems, Zhejiang University, Hangzhou 310058, China*

Abstract: A high-temperature and high-pressure valve is the key equipment of a wind tunnel system; it controls the generation of high-temperature and high-pressure gas. To reduce the adverse impact of high-temperature and high-pressure gas on the strength of the valve body, a cooling structure is set on the valve seat. This can significantly reduce the temperature of the valve body and valve seat. The effects of its structure on the cooling characteristics and stress of the valve seat are studied, and six main parameters that can completely describe the geometry of the cooling structure are proposed. The central composite design method is used to select sample points, and the multi-objective genetic algorithm (MOGA) method is used for optimal structural design. A modification method according to the main parameters for the valve seat is proposed. The results show that the cooling structure weakens the pressure-bearing capability of the valve seat. Among the six main parameters of the valve seat, the distance from the end face of the lower hole to the *Z*-axis and the distance from the axis of the lower hole to the origin of the coordinates have the most obvious effects on the average stress of the valve seat. An optimum design value is proposed. This work can provide a reference for the design of high-temperature and high-pressure valves.

Key words: Control valve; Valve seat; Optimization; Parametric design

1 Introduction

The wind tunnel test is one of the most important means of aerodynamics research in the aerospace field. It simulates the airflow around an aircraft or object by generating and controlling gas. It provides reliable reference data for aircraft design and testing (Formato et al., 2018; Yu et al., 2018; Achuthan and Jayanath, 2021). A high-temperature and high-pressure valve (HTHPV) is the key equipment of a wind tunnel test system. It works in a high-temperature and high-pressure environment, and its main function is to control high-temperature and high-pressure gas in a wind tunnel system (Armijo et al., 2022; Zhou et al., 2022; Aliyeva and Abbasov, 2023; Morales et al., 2023). Owing to the high-temperature and high-pressure conditions, the valve body must have excellent pressure-bearing capacity. If the structural design of the valve body is not efficient, it may negatively affect the life span of the valve and cause economic loss and even casualties. Therefore, it is difficult to overstate the importance of structure optimization of the valve body for an HTHPV to ensure its reliability under extreme conditions (Bryk et al., 2022; Grice et al., 2022).

Thermal stress greatly impacts the pressure-bearing capacity of valves under high-temperature and high-pressure conditions (Shul'zhenko and Kolyadyuk, 2021; Deng, 2022; Li BB et al., 2022; Sundararaj et al., 2022; Qian et al., 2023). The influencing mechanism of thermal stress on valve strength has been considered through experiments (Jawwad et al., 2019), numerical simulations (Bryk, 2022), and theoretical calculations (Hwang et al., 2020). Li WQ et al. (2022) analyzed the valve body stress in the opening process of a feed–water valve by the thermo-fluid-solid coupling method and measured the variation of thermal stress with time. Sun et al. (2021) studied the impact stress of a valve

✉ Wenqing LI, liwenqing@zju.edu.cn
Wenqing LI, https://orcid.org/0000-0001-6228-4772

Received Oct. 28, 2023; Revision accepted Mar. 18, 2024; Crosschecked Dec. 27, 2024

seat at the moment of rapid collision to prevent drawbacks and then optimized the valve seat according to a response surface methodology combined with multi-objective optimization. Fersaoui et al. (2022) evaluated the effect of the thermo-mechanical boundary on the stress of a valve and calculated the thermal stress based on the temperature gradient of each component. Zhang et al. (2021) conducted thermal and structural analyses under transient thermal shock conditions via the thermal–fluid–structure coupling model and reported that, rather than pressure, thermal stress is the main source of stress causing overload accidents in nuclear power plants. Jalali and Delouei (2019) analyzed fatigue and cracks in the stop valve body and compared the stress concentration points obtained with the real coordinates of the crack to evaluate the reliability of the valve body.

Structural optimization is an effective way to improve the performance of a valve (Bao and Wang, 2022). Finding the optimal structural parameters of the valve through relevant optimization algorithms has attracted the attention of many researchers (Li et al., 2020; Kunčická and Kocich, 2022). Zong et al. (2022) proposed a dimensionality-reduced computational fluid dynamics modeling method in which three structural parameters are selected as design variables for structural optimization. Taking a Tesla valve as the research object, Wang et al. (2022) conducted an optimization design, with two structural parameters as input variables and the mixing efficiency and pressure drop as output parameters. Cao et al. (2022) focused on the nonlinearities and parameter uncertainties of a main pressure regulating valve, improving pressure regulation performance via parameter optimization and control methods. Zhang et al. (2022) used a new multi-objective gravitation search algorithm with non-dominated screening and chaos mutation to optimize the pressure regulating valve and revealed the relationships among multiple parameters of the valve. Lin et al. (2022) analyzed the effect of the seal parameters on the seal contact performance of a charge valve and improved the uniformity of the sealing surface by structural optimization. Wang et al. (2021) replaced the Kriging model with the response surface method for greater accuracy and established a combined surrogate model to solve the optimization problem of a butterfly valve.

The above research indicates that reducing the thermal loading is beneficial for improving the bearing pressure ability of HTHPV. The most common method of heat insulation is to install materials with ultralow thermal conductivity, which prevents contact between high-temperature fluid and the inner surface of the valve. The thermal shock of high-temperature fluid on the valve body is not completely eliminated by this method, which leads to an increasing temperature of the valve. This study proposes insulation with a cooling structure. The cooling performance is significantly better than that from installing materials with ultra-low thermal conductivity.

In this paper, the HTHPV is insulated with asbestos between the flow channel of the valve body and the high-temperature and high-pressure gas. The valve body is thus unaffected by high-temperature and high-pressure loads. The temperature of the valve seat increases significantly as the seat is in direct contact with high-temperature and high-pressure gas, leading to the possibility of creep or even structural failure in the seat. Therefore, a cooling structure is required inside the seat, where a coolant can be introduced. The main purpose of this research is to improve the cooling efficiency and structural strength of the valve seat while considering the cooling arrangements. The temperature of the valve seat with different cooling structures under steady-state conditions is analyzed via a numerical simulation method, and the thermal stress of the valve seat is calculated by the thermal-solid coupling method. The cooling structure is represented by six main structural parameters, which are set as independent variables. The average temperature and average thermal stress are selected as target variables. The response surface optimization method is conducted to determine the optimal structural parameters of the valve seat for the best cooling performance and the lowest stress level. This work can provide a reference for the design of HTHPV in the future.

2 Method description

2.1 Geometric model

Fig. 1 shows the structure of the HTHPV, whose size is the same as that of the actual product in the wind tunnel. The HTHPV mainly consists of six parts: a valve cover, a valve stem, a valve core, a valve seat, a valve body, and an inner pipe. The diameter of the inlet and outlet pipes for the HTHPV is 65 mm. The

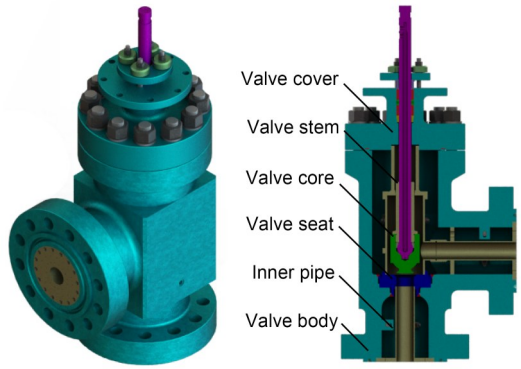

Fig. 1 Geometric model of a high-temperature and high-pressure valve (HTHPV) in a wind tunnel

thermal insulation material is arranged between the valve body and the inner pipe, and the cooling structure is set both in the valve body and the valve seat and can effectively reduce the temperature of the valve body and the valve seat. In this work, the *XOZ* plane is set on the symmetry plane of the valve body, as shown in Fig. 1. To reduce the influence of boundary stress on the calculation results, pipes are added at the inlet and outlet of the HTHPV. The origin of the coordinates is set at the intersection of the axis of the inlet pipe and the outlet pipe.

When the valve is closed, the valve core comes into close contact with the valve seat along the circumferential direction, with no gap between them under preloading. The valve seat, which is welded to the valve body, is connected with the inner pipe and valve core, which includes eight groups of cooling structures along the circumferential direction. Six key parameters of the cooling structure are selected to study the cooling performance. As shown in Fig. 2, D_1 is the diameter of the upper round groove, D_2 is the diameter of the shear hole, D_3 is the diameter of the lower hole, L_1 is the distance from the center of the shear hole to the Z-axis, L_2 is the distance from the end face of the lower hole to the Z-axis, and L_3 is the distance from the axis of the lower hole to the origin of the coordinates. The above six parameters completely describe the geometric characteristics of the cooling structure.

2.2 Mesh and boundary conditions

The mesh of the geometry of the HTHPV is carried out by MESH software in ANSYS WORKBENCH (Canonsburg, PA, USA). The mesh of the HTHPV is shown in Fig. 3. The sweep method is selected to mesh the inlet pipe and outlet pipe, whose grid sizes

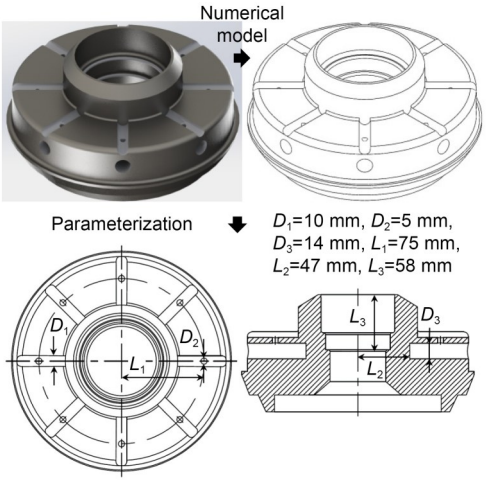

Fig. 2 Geometric model of the valve seat

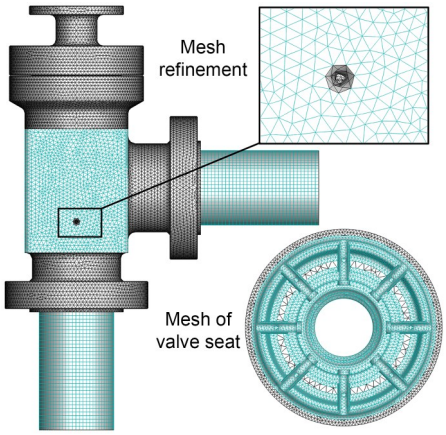

Fig. 3 Mesh of the HTHPV

are both set to 12 mm. A tetrahedron grid is used to generate the mesh of the valve body, valve cover, valve seat, and inner pipe. The gird sizes of the valve seat, inner pipe, valve body, and valve cover are 4 mm, 7 mm, and 12 mm, respectively, with 871070 elements and 1328162 nodes. The contact type between components is bonded. The properties of the solid materials are obtained from ASME BPVC.II.D.M-2021 as listed in Table 1.

Table 1 Material of HTHPV

Part	Material
Valve cover	ASTM A182 F304
Valve stem	X-718/GH3128
Valve core	X-718/GH3128
Valve seat	NS3103/310S
Inner pipe	NS3103/310S
Valve body	ASTM A182 F304

As shown in Fig. 4, there are three main boundary conditions for the temperature calculation for the HTHPV. The contact surface of the valve seat and inner pipe with high-temperature gas is regarded as a convection boundary, the temperature is 600 ℃, and the convection coefficient is 1000 W/(m^2·℃). The surface of the cooling structure is regarded as a convection boundary, the temperature is 22 ℃, and the coefficient is 4500 W/(m^2·℃), which is calculated by the Dittus-Boelter equation. This equation is the longest and most commonly used correlation for forced convection inside pipelines.

$$Nu_{\mathrm{f}}=0.023Re_{\mathrm{f}}^{0.8}Pr_{\mathrm{f}}^{n}, \tag{1}$$

where Nu is the Nusselt number, Re is the Reynolds number, and Pr is the Prandtl number. When the fluid is heated, n=0.4; when the fluid is cooled, n=0.3. The calculation equation for the Nusselt number is as follows:

$$Nu=\frac{hl}{\lambda}, \tag{2}$$

where h is the convective heat transfer coefficient, λ is the thermal conductivity coefficient, and l is the characteristic length.

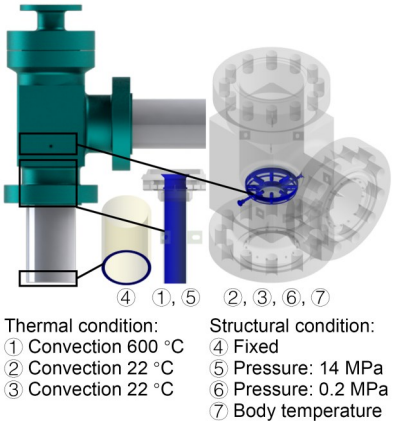

Fig. 4 Boundary conditions of the HTHPV

The calculation equation for the Reynolds number is as follows:

$$Re=\frac{ul}{v}, \tag{3}$$

where u is the fluid velocity, and v is the kinematic viscosity.

The external surface of the HTHPV is regarded as the convection boundary, the temperature is 22 ℃, and the convection coefficient is 15 W/(m^2·℃). For the structural calculation of the HTHPV, there are four main boundary conditions. The contact surface of the valve seat and inner pipe with high-temperature gas is set as the pressure boundary, with a value of 14 MPa. The surface of the cooling structure is set as the pressure boundary; the value is 0.2 MPa. The end surface of the down pipe is a fixed boundary. The temperature distribution of the HTHPV is introduced into the subsequent stress analysis for the HTHPV.

2.3 Optimization method

In this work, as shown in Table 2, the parameters D_1, D_2, D_3, L_1, L_2, and L_3 are set as input parameters, and the parameters T_{ave1}, T_{ave2}, T_{max1}, σ_{max1}, σ_{max2}, σ_{ave1}, and σ_{ave2} are set as output parameters. To fully analyze the effects of structural parameters on the cooling and bearing pressure capacity, the selection range of the input parameters is the limit that can be used to construct geometric entities. To ensure structural integrity, the parameter values are set as shown in Table 3. This paper takes the minimum values of T_{ave1} and σ_{ave1} as the goal of optimization. The central composite design method is selected for the experiments. It provides

Table 2 Descriptions of the input parameters and output parameters

Input parameter	
Parameter	Description
D_1 (mm)	Diameter of the upper round groove
D_2 (mm)	Diameter of the shear hole
D_3 (mm)	Diameter of the lower hole
L_1 (mm)	Distance from center of shear hole to the Z-axis
L_2 (mm)	Distance from end face of lower hole to the Z-axis
L_3 (mm)	Distance from the axis of the lower hole to the origin of coordinates
Output parameter	
Parameter	Description
T_{ave1} (°C)	Average temperature of the valve seat
T_{max1} (°C)	Maximum temperature of the cooling surface
T_{ave2} (°C)	Average temperature of the cooling surface
σ_{max1} (MPa)	Maximum stress intensity of the valve seat
σ_{ave1} (MPa)	Average stress intensity of the valve seat
σ_{max2} (MPa)	Maximum stress intensity of the cooling surface
σ_{ave2} (MPa)	Average stress intensity of the cooling surface

Table 3 Value ranges of the structural parameters of the valve seat

No.	Parameter	Initial value	Range
1	D_1 (mm)	10	9–14
2	D_2 (mm)	5	2–8
3	D_3 (mm)	14	8–14
4	L_1 (mm)	75	65–85
5	L_2 (mm)	47	35–50
6	L_3 (mm)	58	43–58

effective information about experimental variables and experimental errors with minimal test cycles; 45 samples are generated. The screening method is selected for optimization. The genetic aggregation is selected to fit the response surface. A multi-objective genetic algorithm (MOGA) method is used for structural optimization design as a classic multi-objective optimization algorithm. Its basic aim is to solve multi-objective optimization problems within the framework of a genetic algorithm; it uses techniques such as fitness sharing, Pareto front ranking, and crowding distance. The main steps of the MOGA are as follows: population initialization, fitness calculation, Pareto front sorting, crowding distance calculation, selection operation, crossover and mutation operation, population update, and termination condition.

2.4 Verification of the results

A theoretical calculation is carried out to verify the accuracy of the numerical results. The inner pipe of the HTHPV is selected as the object. Its geometry is relatively regular. The inlet pipeline of the valve is considered as a thin-walled cylinder under a uniform internal pressure environment, and its stress is calculated by the force balance principle. The radial stress (X-axis) of the inlet pipe is selected as the reference index. The inner wall radius of the inner pipe is r_1= 32.5 mm, and the outer wall radius of the inner pipe is r_2=36.5 mm. The stress intensity of the inner pipe is calculated by

$$\sigma = \frac{PD}{2t} = \frac{14\times 69}{2\times 4} = 120.5 \text{ MPa}, \tag{4}$$

where P is the pressure, D is the diameter, and t is the wall thickness.

For the numerical calculation, six paths are established, and average stress values are obtained. Fig. 5 shows the comparison between the numerical results and the theoretical results. The maximum stress for the numerical calculation is 123.51 MPa, with a relative error between the numerical and theoretical results of 2.50%. The results of the numerical simulation are consistent with the results of the theoretical calculation and indicate that the numerical method is sufficiently accurate to be used for the structural optimization analysis of the valve seat.

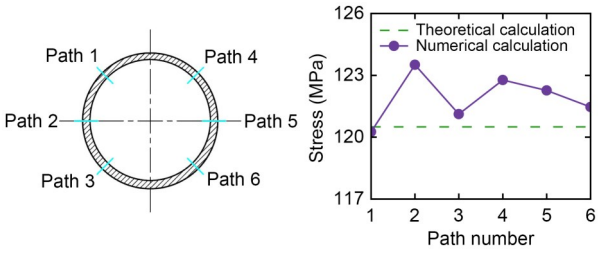

Fig. 5 Comparison between the numerical results and theoretical results

3 Results and discussion

3.1 Temperature and stress analysis

Fig. 6 shows the temperature distribution of the valve seat when the HTHPV is closed. The figure shows that the surface temperature of the valve seat in contact with high-temperature air is the highest, and the temperature around the valve body is relatively low, with a maximum temperature of 242.47 ℃ and a minimum temperature of 22.00 ℃. The temperature of the valve seat decreases from the direction of the central axis to the periphery. Because of the cooling

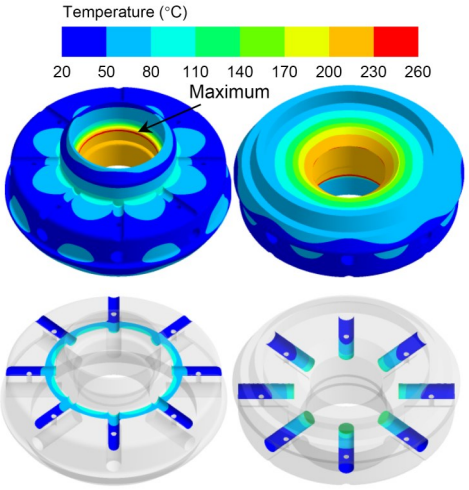

Fig. 6 Temperature distribution of the valve seat

structure, the temperature around the cooling structure is significantly lower than that further away, which shows that the cooling structure has a significant effect on the temperature of the valve seat. The temperature of the end face of the upper round groove is higher than that of the lower hole. In both cases, the temperature near the central axis of the valve seat is higher, whereas the temperature around it is lower.

As shown in Fig. 7, the temperature gradient in the area in contact with high-temperature gas is large. The thermal stress caused by the temperature gradient is also relatively large, which shows that the thermal stress has a significant effect on the stress distribution in the valve seat. The trend of the stress distribution in the valve seat is similar to that of the temperature distribution. The maximum stress occurs in the center hole of the valve seat; its value is 624 MPa. The minimum stress occurs distant from the central hole, and the stress decreases from the central axis of the valve seat to the periphery. The cooling structure causes a stress concentration in the valve seat in this area, especially in the root area of the upper circular groove and the lower hole, which shows that the existence of the cooling structure leads to a weakening of the pressure-bearing capacity of the valve seat.

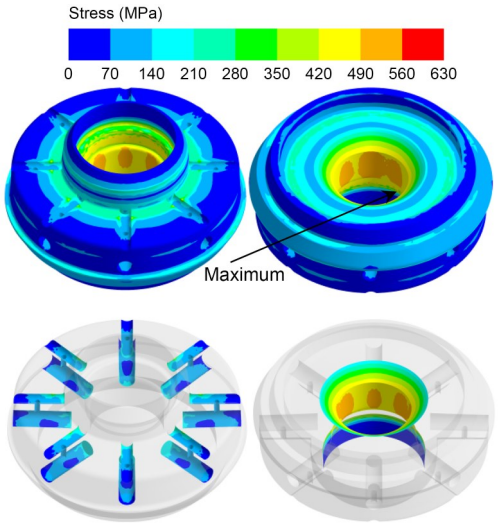

Fig. 7 Stress distribution of the valve seat

3.2 Structural optimization analysis

Fig. 8 shows the local sensitivity of the input parameters (D_1, D_2, D_3, L_1, L_2, and L_3) to the output parameters (T_{ave1}, T_{ave2}, T_{max1}, σ_{max1}, σ_{max2}, σ_{ave1}, and σ_{ave2}) and thus the variation in the output parameters with the

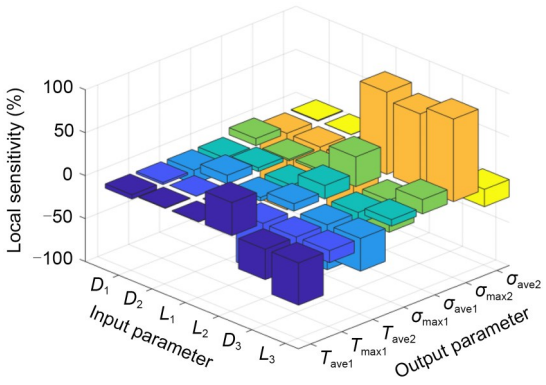

Fig. 8 Responses of the structural parameters to the optimization objectives

input parameters. The parameter that has the greatest influence on the average temperature (T_{ave1}) is the distance from the end face of the lower hole to the Z-axis (L_2). The parameter that has the greatest influence on the average stress intensity (σ_{ave1}) is the distance from the end face of the lower hole to the Z-axis (L_2). The diameter of the lower hole (D_3) and the distance from the axis of the lower hole to the origin of coordinates (L_3) both have significant effects on the average temperature (T_{ave1}). The distance from the end face of the lower hole to the Z-axis (L_2), the diameter of the lower hole (D_3), and the distance from the axis of the lower hole to the origin of coordinates (D_3) all significantly affect the average stress intensity of the cooling surface for the valve seat (σ_{ave2}).

As shown in Fig. 9, when the diameter of the shear hole (D_2) changes from 2 mm to 8 mm, the average temperature of the valve seat (T_{ave1}) generally first increases but then decreases. With the change in D_2, when the distance from the center of the shear hole to the Z-axis (L_1) is between 65 and 72.5 mm, T_{ave1} generally first increases and then decreases; when L_1 is between 72.5 and 80 mm, T_{ave1} shows an "M-type" change trend; when L_1 is between 80 and 85 mm, T_{ave1} first increases and then decreases. When D_2 reaches a minimum or maximum value, the value of T_{ave1} is small. With the continuous increase in L_1, the variation range of T_{ave1} with D_2 increases. When $D_2 \leqslant 2$ mm or $D_2 \geqslant 7$ mm and $L_1 \geqslant 80$ mm, L_1 is relatively small, which provides a way to reduce the average valve seat temperature (T_{ave1}).

Fig. 10 shows the variation trend of average temperature of the valve seat (T_{ave1}) with the distance from the end face of the lower hole to the Z-axis (L_2) and the

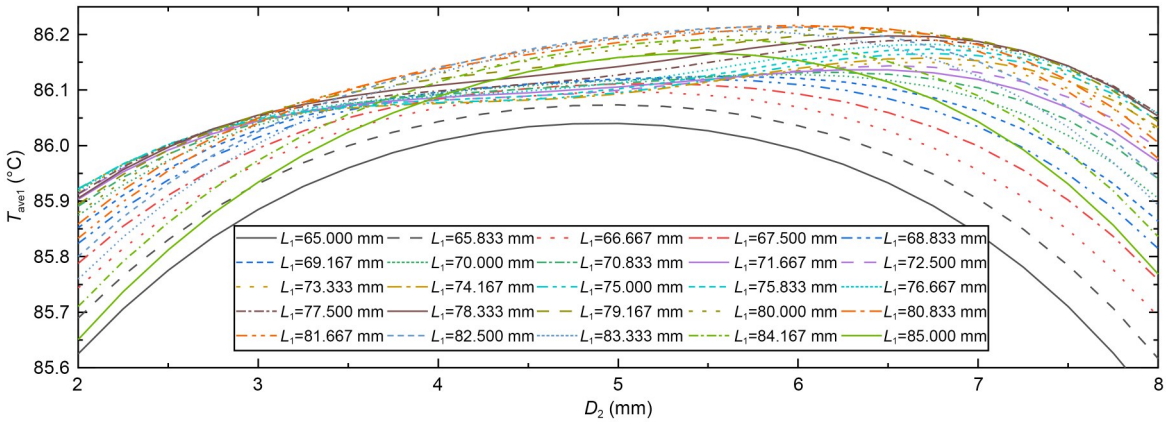

Fig. 9 Responses of parameters D_2 and L_1 to optimization target T_{ave1}. References to color refer to the online version of this article

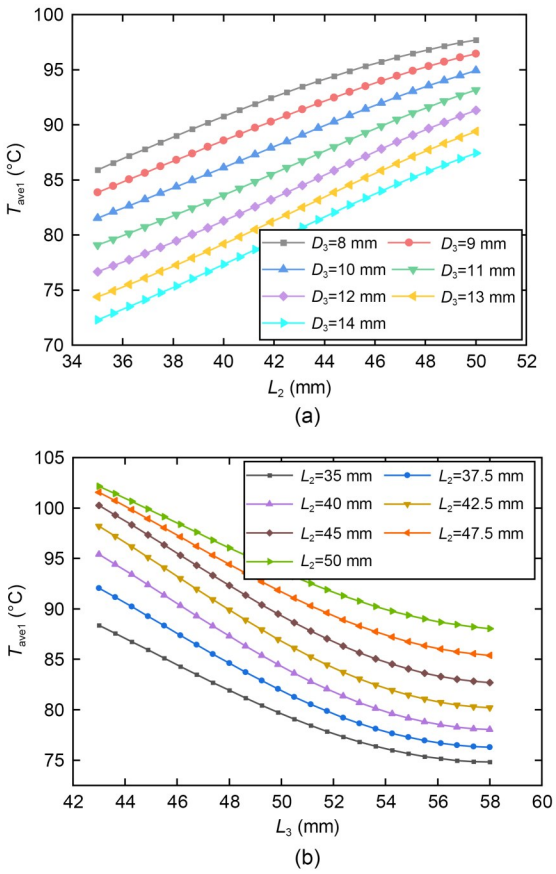

Fig. 10 Responses of parameters L_2 (a) and L_3 (b) to optimization target T_{ave1}. References to color refer to the online version of this article

distance from the axis of the lower hole to the origin of the coordinates (L_3). When the diameter of the lower hole (D_3) remains unchanged, T_{ave1} increases with the increase of L_2. When L_2 remains unchanged, T_{ave1} decreases with the increase of D_3. Therefore, reducing L_2 and increasing parameter D_3 can effectively reduce the value of T_{ave1}. When L_2 remains unchanged, T_{ave1} decreases with the increase of L_3. When $L_3 \leqslant 52$ mm, the decrease range of T_{ave1} is large, and when $L_3 > 52$ mm, the decrease range of T_{ave1} is small. When L_3 remains unchanged, T_{ave1} also increases with the continuous increase in L_2. Therefore, increasing L_3 and reducing L_2 can also effectively reduce the value of T_{ave1}.

Fig. 11 shows the response surface of average temperature of the valve seat (T_{ave1}) with the diameter of the upper round groove (D_1) and the diameter of the shear hole (D_2). When D_2 remains unchanged, T_{ave1} decreases with the increase of D_1. When D_1 remains unchanged, T_{ave1} first increases and then decreases with the increase of D_2. Therefore, increasing D_1 and $D_2 \leqslant 3$ mm or $D_2 \geqslant 7$ mm can reduce the value of T_{ave1} slightly.

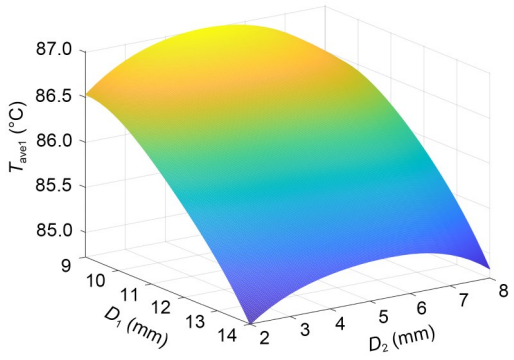

Fig. 11 Responses of parameters D_1 and D_2 to T_{ave1}

Fig. 12 shows the variation trend of the average stress intensity of the valve seat (σ_{ave1}) with the diameter of the upper round groove (D_1) and the diameter of the shear hole (D_2). When $D_2 \leqslant 5$ mm, σ_{ave1} increases

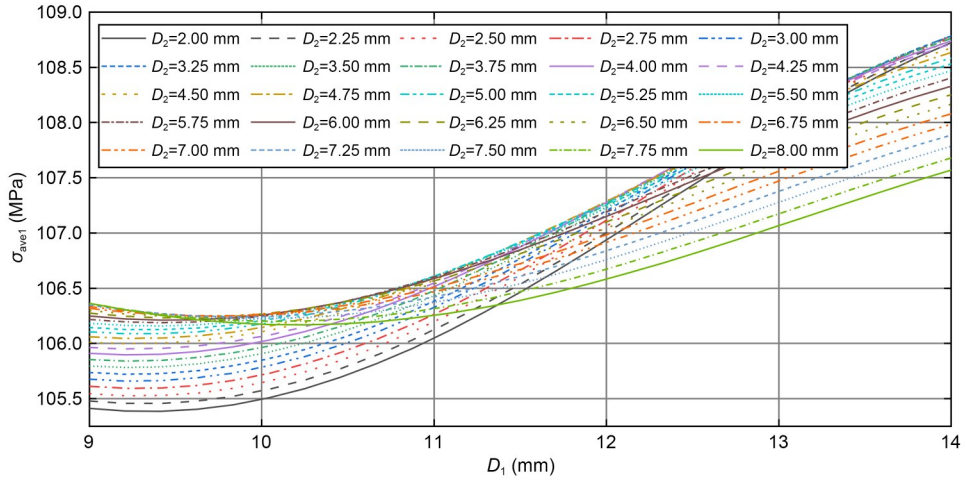

Fig. 12 Responses of parameters D_1 and D_2 to optimization target σ_{ave1}. References to color refer to the online version of this article

with the increase of D_1. When $D_2 \geqslant 5$ mm, σ_{ave1} decreases first and then increases with the increase of D_1. It should be noted that when $D_1 \leqslant 12.5$ mm, the change range of σ_{ave1} is small, and when $D_1 \geqslant 12.5$ mm, the change range of σ_{ave1} is relatively large. When D_1 is small, the value of σ_{ave1} increases with the increase of D_2. When D_1 is large, the value of σ_{ave1} decreases with the increase of D_2. Decreasing D_2 while reducing D_1 can effectively reduce the value of σ_{ave1}.

Fig. 13 shows the variation trend of the average stress intensity of the valve seat (σ_{ave1}) with the diameter of the upper round groove (D_1) and the diameter of the shear hole (D_3). When $L_2 \leqslant 40$ mm, with the increase of D_1, parameter σ_{ave1} first decreases and then increases. When $L_2 > 40$ mm, σ_{ave1} first increases and then decreases with the increase of D_1. When D_1 remains unchanged, σ_{ave1} increases with the increase of parameter L_2. This shows that when D_1 is 11–12 mm and $L_2 \leqslant$ 10 mm, the value of σ_{ave1} can be effectively reduced. When $L_3 \leqslant 55.5$ mm, with the increase of D_3, σ_{ave1} also shows an M-type change trend, which shows that when D_3=14 mm and $L_3 \leqslant 55.5$ mm, the value of σ_{ave1} is the smallest.

In Fig. 14, the response surfaces of the average stress intensity of the valve seat (σ_{ave1}) with the distance from the center of the shear hole to the Z-axis (L_1) and the distance from the end face of the lower hole to the Z-axis (L_2) are shown. When L_1 remains invariable, σ_{ave1} increases with the increase of L_2. When L_2 remains unchanged, σ_{ave1} increases with the increase of L_1. Therefore, the value of σ_{ave1} can be reduced slightly by decreasing L_2 and reducing L_1.

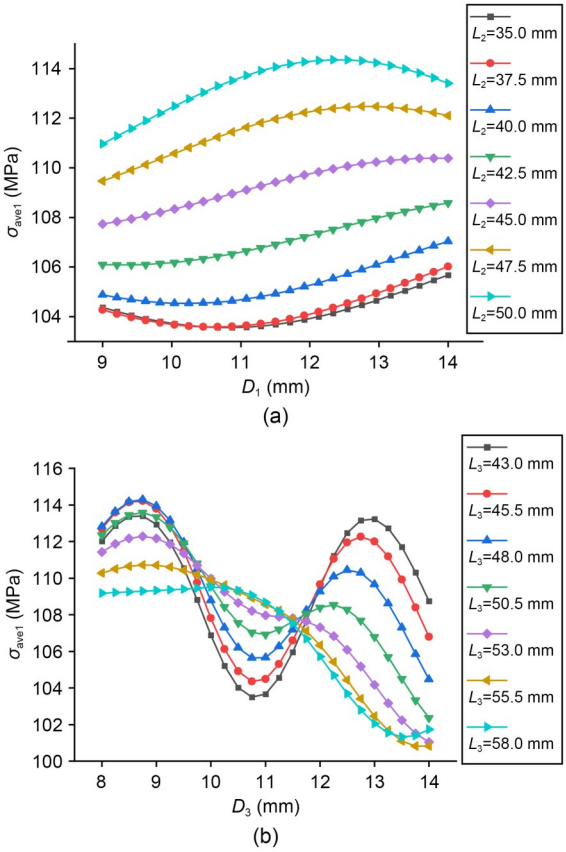

Fig. 13 Responses of parameters D_1 (a) and D_3 (b) to optimization target σ_{ave1}. References to color refer to the online version of this article

Fig. 15 shows the response surface of the average stress intensity of the valve seat (σ_{ave1}) with the diameter of the shear hole (D_2) and the distance from the axis of the lower hole to the origin of the coordinates (L_3).

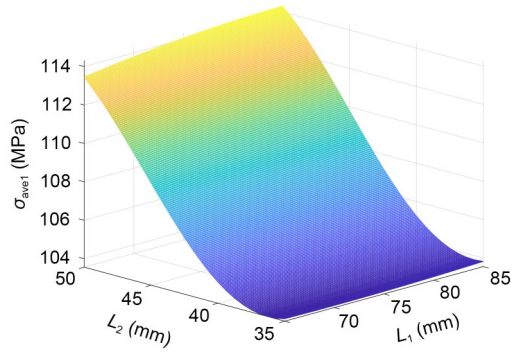

Fig. 14 Responses of parameters L_1 and L_2 to optimization target σ_{ave1}

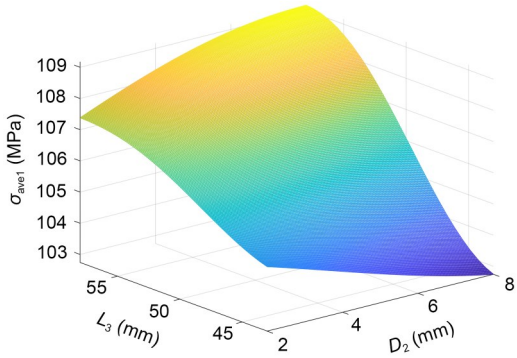

Fig. 15 Responses of parameters D_2 and L_3 to optimization target σ_{ave1}

When D_2 remains unchanged, σ_{ave1} decreases with the decrease of L_3. When $L_3 \leqslant 50$ mm, σ_{ave1} falls off with the increase of parameter D_2. When $L_3 > 50$ mm, σ_{ave1} is augmented with the increase of D_2. Therefore, increasing D_2 and decreasing L_3 can reduce the value of σ_{ave1} slightly.

At the values of D_1–D_3 and L_1–L_3 shown in Table 4, the average temperature of the valve seat can be reduced from 242.47 °C to 70.61 °C, and the average stress of the valve seat can be reduced from 115.22 MPa to 100.02 MPa, which shows that the cooling performance of the valve seat has been greatly improved and that security is guaranteed.

Table 4 Optimization results of the structural parameters for the optimization value

Parameter	Initial value	Final value
D_1	10 mm	11.90 mm
D_2	5 mm	2.81 mm
D_3	14 mm	13.83 mm
L_1	75 mm	74.78 mm
L_2	47 mm	36.06 mm
L_3	58 mm	54.95 mm
T_{ave1}	242.47 °C	70.61 °C
σ_{ave1}	115.22 MPa	100.02 MPa

4 Conclusions

When the HTHPV is closed, the temperature around the cooling structure is significantly lower than that away from the area because of the existence of the cooling structure. The temperature of the area in contact with high-temperature air is significantly higher than that of the surrounding area.

The stress distribution of the valve seat is similar to that of the temperature. The maximum stress appears at the center hole of the valve seat, the minimum stress appears at the position far away from the center hole, and the stress distribution decreases from the center axial direction of the valve seat. The existence of the cooling structure causes a stress concentration of the valve seat in this area, especially in the root area of the upper circular groove and the lower hole, which shows that the existence of the cooling structure weakens the pressure-bearing capacity of the valve seat.

An optimization method based on the cooling structure parameters is proposed, which can completely describe the geometric characteristics of the cooling structure and improve the cooling performance. Through the central composite design method and screening optimization method, the influence of various parameters on the optimization objective is analyzed. The distance from the end face of the lower hole to the Z-axis (L_2) has the most obvious effect on the average temperature of the valve seat (T_{ave1}). The distance from the end face of the lower hole to the Z-axis (L_2) and the distance from the axis of the lower hole to the origin of the coordinates (L_3) have the most obvious effects on the average stress intensity of the valve seat (σ_{ave1}). Finally, an optimal design value is proposed in which the average temperature of the valve seat can be reduced from 242.47 °C to 70.61 °C and the average stress of the valve seat can be reduced from 115.22 MPa to 100.02 MPa.

Acknowledgments

This work is supported by the National Natural Science Foundation of China (No. 52175067), the Zhejiang Key Research & Development Project (No. 2021C01021), the Natural Science Foundation of Zhejiang Province (No. LY20E050016),

and the Postdoctoral Fellowship Program of China Postdoctoral Science Foundation (CPSF) (No. GZC20241478).

Author contributions

Fengwei HOU designed the research. Haifeng SHU and Binbin WU processed the corresponding data. Wenqing LI wrote the first draft of the manuscript. Chengliang YU and Zhehui MA helped to organize the manuscript. Fengwei HOU and Jinyuan QIAN revised and edited the final version.

Conflict of interest

Fengwei HOU, Haifeng SHU, Binbin WU, Chengliang YU, Zhehui MA, Wenqing LI, and Jinyuan QIAN declare that they have no conflict of interest.

References

Achuthan A, Jayanath S, 2021. Stress analysis of variable ram blowout prevention valves. *SPE Drilling & Completion*, 36(3):647-657. https://doi.org/10.2118/205348-PA

Aliyeva SY, Abbasov SH, 2023. Determination of the friction force between the draw rod and its guide in sucker rod well pumps and an analytical study of the stress deformation state of the valve assembly. *Nafta-Gaz*, 79(9):596-603. https://doi.org/10.18668/NG.2023.09.05

Armijo KM, Mendoza H, Parish J, 2022. Vapor transport analysis of a chloride molten salt flow control valve. *AIP Conference Proceedings*, 2445(1):020001. https://doi.org/10.1063/5.0085644

Bao YH, Wang HG, 2022. Numerical study on flow and heat transfer characteristics of a novel Tesla valve with improved evaluation method. *International Journal of Heat and Mass Transfer*, 187:122540. https://doi.org/10.1016/j.ijheatmasstransfer.2022.122540

Bryk M, 2022. Thermal-strength analysis of a slow closing valve during accelerated startup of a steam turbine. *Journal of Power Technologies*, 102(2):68-78.

Bryk M, Banaszkiewicz M, Kowalczyk T, et al., 2022. Slowly-closing valve behaviour during steam machine accelerated start-up. *Case Studies in Thermal Engineering*, 39:102457. https://doi.org/10.1016/j.csite.2022.102457

Cao G, Wu HC, Chu YM, et al., 2022. Optimal design and dynamic optimization of the main pressure regulating valve for heavy-duty automatic transmission using GA and PSO algorithms. *Journal of the Brazilian Society of Mechanical Sciences and Engineering*, 44(3):94. https://doi.org/10.1007/s40430-022-03370-9

Deng X, 2022. Computational Analysis of Turbulence and Thermal Characteristics in Fluid Film Thrust Bearings. PhD Thesis, University of Virginia, Charlottesville, USA.

Fersaoui B, Cerdoun M, May A, et al., 2022. Thermo-mechanical stress analysis within a steel exhaust valve of an internal combustion engine. *Proceedings of the Institution of Mechanical Engineers, Part C: Journal of Mechanical Engineering Science*, 236(1):635-654. https://doi.org/10.1177/0954406221996394

Formato A, Guida D, Ianniello D, et al., 2018. Design of delivery valve for hydraulic pumps. *Machines*, 6(4):44. https://doi.org/10.3390/machines6040044

Grice D, Hanke L, Mathias J, 2022. Analysis of stop valve leaks: environmental stress cracking of styrene copolymer valve stems. *Journal of Failure Analysis and Prevention*, 22(2): 666-675. https://doi.org/10.1007/s11668-022-01364-2

Hwang SY, Kim MS, Lee JH, 2020. Thermal stress analysis of process piping system installed on LNG vessel subject to hull design loads. *Journal of Marine Science and Engineering*, 8(11):926. https://doi.org/10.3390/jmse8110926

Jalali A, Delouei AA, 2019. Failure analysis in a steam turbine stop valve of a thermal power plant. *Engineering Failure Analysis*, 105:1131-1140. https://doi.org/10.1016/j.engfailanal.2019.07.057

Jawwad AKA, Mahdi M, Alshabatat N, 2019. The role of service-induced residual stresses in initiating and propagating stress corrosion cracking (SCC) in a 316 stainless steel pressure-relief-valve nozzle set. *Engineering Failure Analysis*, 105:1229-1251. https://doi.org/10.1016/j.engfailanal.2019.07.062

Kunčická L, Kocich R, 2022. Effects of temperature (in)homogeneity during hot stamping on deformation behavior, structure, and properties of brass valves. *Advanced Engineering Materials*, 24(7):2101414. https://doi.org/10.1002/adem.202101414

Li BB, Li RR, Liu XM, et al., 2022. Effects of operating parameters on flow force characteristics in a conical throttle valve. *Industrial Lubrication and Tribology*, 74(2):251-257. https://doi.org/10.1108/ILT-12-2020-0452

Li JF, Xiao MQ, Sun Y, et al., 2020. Failure mechanism study of direct action solenoid valve based on thermal-structure finite element model. *IEEE Access*, 8:58357-58368. https://doi.org/10.1109/ACCESS.2020.2982941

Li WQ, Zhao L, Yue Y, et al., 2022. Thermo-mechanical stress analysis of feed-water valves in nuclear power plants. *Nuclear Engineering and Technology*, 54(3):849-859. https://doi.org/10.1016/j.net.2021.09.018

Lin ZH, Yu LJ, Hua TF, et al., 2022. Seal contact performance analysis of soft seals on high-pressure hydrogen charge valves. *Journal of Zhejiang University-SCIENCE A (Applied Physics & Engineering)*, 23(4):247-256. https://doi.org/10.1631/jzus. A2100395

Morales LLD, Silva GP, Barros LDO, et al., 2023. Damage to fracture in offshore engineering materials under several stress states: blowout preventer valve application. *Advances in Structural Engineering*, 26(11):2025-2054. https://doi.org/10.1177/13694332231182862

Qian JY, Xu JX, Zhong FP, et al., 2023. Solid-liquid flow characteristics and sticking-force analysis of valve-core fitting clearance. *Journal of Zhejiang University-SCIENCE A (Applied Physics & Engineering)*, 24(12):1096-1105. https://doi.org/10.1631/jzus.A2300061

Shul'zhenko MG, Kolyadyuk AS, 2021. Thermal strength of steam turbine shut-off and control valves body. *Strength of Materials*, 53(6):877-888.

https://doi.org/10.1007/s11223-022-00355-w

Sun B, Zhao T, Kurnianto Prayitno YA, et al., 2021. Optimization of design variables for rotary regenerative thermal oxidizer high-temperature valve (*rto*-HTV) based on transient dynamics analysis and multi-objective optimization algorithm. *AIP Advances*, 11(12):125312. https://doi.org/10.1063/5.0075307

Sundararaj S, Krishnakumar P, Anirudh VR, et al., 2022. Effect of water pressure and temperature on spherical float of level sensing auto drain valve. *Materials Today: Proceedings*, 49: 1490-1497. https://doi.org/10.1016/j.matpr.2021.07.235

Wang HL, Chen XY, 2022. Optimization of micromixer based on an improved Tesla valve-typed structure. *Journal of the Brazilian Society of Mechanical Sciences and Engineering*, 44(4):143. https://doi.org/10.1007/s40430-022-03454-6

Wang LT, Zheng SK, Liu X, et al., 2021. Flow resistance optimization of link lever butterfly valve based on combined surrogate model. *Structural and Multidisciplinary Optimization*, 64(6):4255-4270. https://doi.org/10.1007/s00158-021-03060-5

Yu KK, Xu JL, Liu S, et al., 2018. Starting characteristics and phenomenon of a supersonic wind tunnel coupled with inlet model. *Aerospace Science and Technology*, 77:626-637. https://doi.org/10.1016/j.ast.2018.03.050

Zhang H, Zhao L, Peng SE, et al., 2021. Thermal-fluid-structure analysis of fast pressure relief valve under severe nuclear accident. *Nuclear Engineering and Design*, 371:110937. https://doi.org/10.1016/j.nucengdes.2020.110937

Zhang TY, Zhou JZ, Yang X, et al., 2022. Multi-objective optimization and decision-making of the combined control law of guide vane and pressure regulating valve for hydroelectric unit. *Energy Science & Engineering*, 10(2):472-487. https://doi.org/10.1002/ese3.1038

Zhou X, Zhi XQ, Gao X, et al., 2022. Cavitation evolution and damage by liquid nitrogen in a globe valve. *Journal of Zhejiang University-SCIENCE A (Applied Physics & Engineering)*, 23(2):101-117. https://doi.org/10.1631/jzus. A2100168

Zong CY, Li QY, Li KP, et al., 2022. Computational fluid dynamics analysis and extended adaptive hybrid functions model-based design optimization of an explosion-proof safety valve. *Engineering Applications of Computational Fluid Mechanics*, 16(1):296-315. https://doi.org/10.1080/19942060.2021.2010602